American Journal of Nanotechnology & Nanomedicine

Research Article

Sono and Photo Sensitized Gallium-Porphyrin Nanocomposite in Tumor-Bearing Mice: new Concept of Cancer Treatment -

Samir Ali Abd El-Karem[1]*, Gihan Hosny Abd Elsamie[2] and Abtisam Jasim Abbas[2,3]

[1]*Department of Applied Medical Chemistry, Medical Research Institute, Alexandria University, Egypt*

[2]*Division of Environmental Health, Dept. of Environmental Studies, Institute of Graduate Studies and Research, Alexandria University, Egypt*

[3]*College of Science, University of AL-Qadisiyah, Iraq*

***Address for Correspondence:** Samir Ali Abd El-Karem, Department of Applied Medical Chemistry, Medical Research Institute, Alexandria University, Egypt, Tel: +012-838-262-75; ORCID ID: orcid.org/0000-0003-4899-9338; E-mail: Samir_ali852006@yahoo.com

Submitted: 17 February 2019 **Approved:** 02 March 2019 **Published:** 05 March 2019

Cite this article: El-Karem SAA, Abd Elsamie GH, Abbas AJ. Sono and Photo Sensitized Gallium-Porphyrin Nanocomposite in Tumor-Bearing Mice: new Concept of Cancer Treatment. Am J Nanotechnol Nanomed. 2019; 2(1): 005-0013.

ABSTRACT

This study was directed at study the effectiveness of cancer targeted therapy using the activated Gallium-Porphyrin Nanocomposite (Nano-GaP). Study was applied on male Swiss albino mice, implanted with Ehrlich Tumor (EAC) divided into six groups. Two energy sources were used; laser and ultrasound. Results showed that Nano-GaP is a potential sensitizer for photodynamic or sonodynamic treatment of tumor. Nano-GaP plays an important role in tumor growth inhibition and cell death induction. Activated Nano-GaP with both infrared laser and ultrasound has a potential antitumor effect. The results indicated that Folic Acid-Nanographene Oxide-Gallium-Porphyrin Nanocomposite (FA–NGO–GaP) could be used as a unique nanocomposite for cancer targeted Sono-Photodynamic Therapy (SPDT).

Keywords: Nano-gallium-porphyrin; Sonodynamic therapy; Photodynamic therapy

INTRODUCTION

Cancer is the major cause of death worldwide. During 2012, there were 14 million new cancers and 8 million cancer decease worldwide and by 2030, the cosmopolitan burden is predictable to reach to 22 million incoming cancer patients and 13 million cancer decease [1-3]. Current treatments used for cancer treatment include surgery, chemotherapy, and radiotherapy. Despite these treatments have been practiced and accepted for decades, they have their disadvantages and unfavorable effects. Removal of tumors by surgery is limited to large tumors and is available. Chemotherapy drugs target rapidly proliferating cells, so killing not only cancer cells but also destroying normal cells such as bone marrow cells and immune cells. These lead to extensive "collateral damage" in the patient's body. Radiotherapy involves the use of high-energy rays such as x-rays and rays to either destroy cancer cells, which inevitably leads to harmful effects on healthy tissue along the path of radiation. It is clear that the need for advanced technology to play an important role in cancer treatment is clear in statistics indicating that rates of cancer incidence, mortality and mortality are still at very high levels [4,5].

In recent years, there has been increasing interest in using of Photodynamic Therapy [PDT] to treat different types of cancers, either on its own or in combination with other anticancer treatment methods. PDT involve the administration of a Photosensitizing (PS) drug and subsequently illuminating the target area with light corresponding to the absorbance wavelength of the PS, triggering a series of biological effects [5-8].

Sonodynamic Therapy [SDT] has been raised as a promising noninvasive approach derived from PDT. The low penetration depth of light, PDT is not effective for the treatment of deep tumors. A great advantage of SDT on a PDT is that it can penetrate soft tissue up to tens of centimeters therefore; SDT overcomes the limitation of PDT [9-12].

Sono-Photodynamic Therapy [SPDT] is a new therapeutic method that utilizes a safe agent with sono and photo sensitive properties. PDT and SDT have been applied for years as separate processes for the treatment of cancer with variable results. PDT alone is used for more superficial tumor, but when combined with SDT; it has been shown to be efficient for deep-seated as well as metastatic tumors [13].

Gallium-porphyrin; GaP or [7, 12 - bis (1 - decyloxyethyl) - Ga (III) - 3, 8, 13, 17 – tetramethylporphyrin - 2, 18 – dipropionyldiaspartic acid] is one of the metal-deuteroporphyrin complexes as SPS for SPDT, the gallium complexes exhibit long phosphorescence lifetime. This long phosphorescence lifetime can be of a great advantage in the efficient generation of singlet oxygen to induce significant tumor tissue destruction.

The aim of this work was to study the effectiveness of nano-gallium-porphyrin in activated cancer-targeted therapy. To achieve our goal the following was done:

MATERIALS AND METHODS

Synthesis of Nanographene Oxide (NGO), conjugation of Folic Acid with Nanographene Oxide (FA-NGO) and photosensitizer gallium-porphyrin loading on FA-NGO (FA-GO-GaP) according to Abd El-Kaream SA, et al. [14]. In the present work gallium-porphyrin was used as sono-photosensitizer; chemically active by absorption of light and/or ultrasound. Gallium-porphyrin was purchased from Molbase Chemicals Co. India. The sono-photosensitizer obtained as powder stored in dark bottle at -20°C temperature and with purity: 99.9% by HPLC analysis. GaP was dissolved in a sterilized phosphate buffer saline solution with pH = 7.4 and mixed with FA-NGO (0.5 mg/ mL) at room temperature for 24 h. The loading efficiency of GaP was approved using UV absorbance at 663 nm. FA-NGO-GaP administered to tumor-bearing mice Intraperitoneal (IP) injection for 15 days 18-20 hours before exposure to either photo and/or sonodynamic treatment modality.

Experimental design and tumor implantation

This study was conducted on one hundred and thirty male Swiss albino mice. Ehrlich ascites carcinoma tumor cells, 2 x 106 human female mammary cells in origin, diluted approximately ten times in 0.9% saline were inoculated subcutaneously on the left abdominal region of mice purchased from national cancer institute, Cairo University. The animals were housed in plastic cages and were kept under natural light with diet and water at available. When tumors reach to 10 mm in diameter on day 10 after implantation, the treatment study was started. Use of experimental animals in the study protocol was carried out in accordance with the ethical guidelines of the medical research institute, Alexandria University (Guiding Principles for Biomedical Research Involving Animals, 2011). Mice were grouped into the following:

*__Group I:__ (30 mice); a) 10 mice: Control without tumor, b) 10 mice: Tumor bearing mice without treatment, c) 10 mice: Tumor bearing mice treated with (FA-NGO-GaP) only.

*__Group II:__ (20 mice, laser irradiated group); a) 10 mice: were exposed to Infra-Red Laser, 4000Hz, for 3 minutes, b) 10 mice: were exposed to Infra-Red Laser, 7000Hz, for 3 minutes.

*__Group III:__ (20 mice, ultrasound group); a) 10 mice: were exposed to pulsed ultrasound for 3 minutes, b) 10 mice: were exposed to continuous ultrasound for 3 minutes.

*__Group IV:__ (20 mice, (FA-NGO-GaP), laser group); Tumor bearing mice of this group were injected (IP) with (FA-NGO-GaP),

then the tumor sites were irradiated to laser light at same conditions of group II.

*Group V: (20 mice, (FA-NGO-GaP), ultrasound group); Tumor bearing mice of this group were injected (IP) with (FA-NGO-GaP), then were divided into 2 sub-groups. The tumor sites were irradiated to ultrasound at same conditions of group III.

*Group VI: (20 mice, combined treatment groups); a) 10 mice: were irradiated to laser light for 3 minutes, followed by ultrasound for 3 minutes, b) 10 mice: Injected (IP) with (FA-NGO-GaP), then tumor sites were irradiated to laser light (7000 Hz) for 3 min, followed by pulsed ultrasound for 3 minutes.

Laser/ ultrasound exposure

For laser and/or ultrasound exposure, the mice were anesthetized with diethyl ether. The hair over the tumors was shaved off. The mice were fixed on a board with the tumor upwards. The probe was placed nearly on the tumor, which was irradiated with laser and/or ultrasound for 3 minutes at the different conditions as mentioned before. After PDT, SDT and SPDT, animals were maintained in the dark to avoid skin irritation. Exposure of mice tumor to the laser beam was carried out using an Infrared diode laser, model LAS 50-Hi-Tech fysiomed, Germany operated at a wavelength of 904 nm and a peak power of 50 W at a frequency up to 7000 Hz. Exposure of mice tumor to the continuous and pulsed ultrasound was carried out using an ultrasonic therapy instrument (Model CSl Shanghai, No. 822 Factory. China). This instrument uses electronic tube to generate an electric oscillation with frequency 0.8 MHz and power output which converted to ultrasonic mechanical energy by means of ultrasonic transducer (calcium zirconate –titanate). The mechanical ultrasonic energy has a beam power density which can be adjusted from 0.5 to 3W/cm^2. This instrument operates at both continuous wave mode with output power from 0.5 - 3W/ cm^2 adjustable in 11 steps and pulsed mode (pulse frequency 1000 Hz, duty ratio 1/3 and average power density from 0.15-1 W/ cm^2). For evaluation of the treatment effects to all studied groups the following investigations were done:

Tumor growth/ inhibition assay

During treatment session, tumor growth was examined regularly every day. Length and width of tumors were measured with a slide caliper and tumor volume (in mm^3) was calculated by the use of the following equation.

TV (mm^3) = 22/7x4/3x (length/2) x (width/2)^2

Two weeks after the treatment, the mice were sacrificed and the tumors were dissected out, weighed (in grams). The tumor volume growth ratio and tumor mass inhibition ratio were calculated as follows.

TMIR = 1- (average tumor weight of treated group/ average tumor weight of control group) x100

Biochemical examination

Blood sample (2.5 ml of venous blood) was withdrawn from all mice group. This blood samples were allowed to clot thoroughly for 20 minutes then centrifuged at 3000 x g for 20 minutes for separating serum for biochemical examinations. All biochemical analysis was done on Indiko Plus Auto-analyzer.

Oxidative stress and antioxidant profile: Lipid peroxidation (MDA) assay kit (BioVision Catalog # K739-100), Total Antioxidant Capacity (TAC) assay kit (BioVision Catalog #K274-100), Glutathione Reductase (GR) activity assay kit (BioVision Catalog #K761-100), Glutathione-S-Transferase (GST) activity assay kit (BioVision Catalog #K263-100), Superoxide Dismutase (SOD) activity assay kit (BioVision Catalog #K335-100), Catalase (CAT) activity assay kit (BioVision Catalog #K773-100), were used according to the manufacturer's instructions.

Kidney and liver biomarkers: Urea (Sigma Catalog # MAK179), creatinine (Sigma Catalog # MAK080), Alanine Transaminase (ALT) Activity Assay Kit (Sigma Catalog # MAK052), Aspartate Aminotransferase (AST) Activity Assay Kit (Sigma Catalog #MAK055) and γ-Glutamyl Transferase (GGT) Activity Assay Kit (Sigma Catalog #MAK089), were used according to the manufacturer's instructions.

Molecular detection of osteopontin mRNA gene expression in excised tumor *via* RT-PCR: RNA was extracted from the Erich tumor of mice using QIAamp RNA tissue kit, was purchased from QIAGEN, USA according to the manufacturer's instructions. Preparation of Full-Length First strand cDNA from RNA template using RevertAid TM First cDNA Strand Synthesis Kit. Reverse transcription reaction was carried out in a 20 µl reaction mixture by using RevertAid TM First cDNA Strand Synthesis Kit # K1621, #1622, was purchased from MBI Fermentas, Lithuania according to manufacturer's instruction. For amplification; to each PCR tube the following were added 5 µl (0.25 µg) Template osteopontin - cDNA, 10 µl Taq TM Green PCR Master Mix (2X) {dNTPs [0.4 mM of each dATP, dCTP, dGTP, dTTP], 0.05u/µl Taq DNA polymerase and reaction buffer} # k1081, was purchased from MBI Fermentas, Lithuania, 1.5 µl osteopontin forward primer: 5µ-CTT TCACTC CAATCGTCCCTA C-3, 1.5 µL osteopontin reverse primers: 5-GCTCTC TTTGGAATGCTCAAGT-3 and deionized-RNase free water to final volume 20 µl. The reaction mixtures were gently vortexed, briefly centrifuged to collection all drops to the bottom of the tubes, then were placed in the thermal cycler (Little Genius, Bioer Co), The PCR mixture was subjected to 35 amplification cycles. PCR thermal profile was as follow: pre-denaturation (94°C, 2min), followed by 35 cycles of denaturation (94°C, 1min), annealing (52°C, 1min), and extension (72°C, 1min), with a final extension (72°C, 7min). To verify the successful preparation of mRNA and as positive controls, samples were detected for the presence of Glyceraldehyde-3-Phosphate Dehydrogenase (GAPDH) mRNA. Forward primer: 5-AGGCCGGTGCTGAGTATGTC-3, reverse primers: 5-TGCCTGCTTCACCACCTTCT-3. Reaction tubes containing no cDNA control template and without cDNA sample addition were included as negative controls for each PCR reaction. For detection; Amplicons were analyzed with 2% (wt/ vol) ethidium bromide stained agarose gel. The bands were visualized on a 302 nm UV transilluminator (BIO-RAD, USA).The gel was examined for bands of 305bp and 530bp as determined by the molecular weight marker (Gene Ruler TM 100bp DNA marker #SM0323, was purchased from Fermentas, Lithuania) runs at the same time and then photographed using a digital camera .

Histopathological examination

Small pieces of Ehrlich tumor tissue of the experimental groups were processed and examined by Haematoxylin and Eosin (H&E) method as follows; small pieces of Ehrlich Tumor tissues were fixed at 10% formaldehyde, dehydrated in ascending grades using alcohol, embedded in paraffin to produce paraffin block, the blocks were cut

into 3-4 µm thick sections and floated in water bath, cleaned with xylene, rehydrated in descending grades of alcohol, stained with haematoxylin and eosin stain, cleaned again ethylene and covered by covering slides, thus the slides were prepared to be examined by light microscopy.

STATISTICAL ANALYSIS OF DATA

The findings were presented using One-Way Variance Analysis (ANOVA). Results were expressed as mean ± Standard Deviation (SD) and values of $P > 0.05$ were considered non-significantly different, while values of $P < 0.05$ were assumed significant. F probability expresses the general effect between groups.

RESULTS

Treatment with NGaP without activation has little or no effect on tumor volume and tumor weight. Up to one week, all treatment modulates have little effect on the tumor volume and tumor weight. After one week, treatment with IRL and ultrasound (pulsed or continuous wave) in the presence or absence of NGaP, become more effective. The presence of NGaP increases the effect of both IRL and ultrasound. Results obtained indicated that pulsed ultrasonic wave is more effective than continuous ultrasonic wave in the presences of NGaP. Pulsed wave ultrasound at 3W/ cm^2 was selected to combine with IRL at 7000 Hz. This combined treatment modality is more effective on tumor cells than using of Infrared Laser (IRL) or ultrasound alone (Figure 1-3).

Oxidative stress and antioxidant profile

In our study, the increase in lipid peroxidation was reported in controlled group which carried EAC. In all the irradiated groups and that irradiated and treated without NGaP, a significant increase in the levels of MDA was observed. Animals in groups irradiated with IRL or U.S or both with NGaP exhibited significantly low levels of MDA, as compared with the cancer control group or with treated mice without activation of NGaP, (Figure 4). The same table, the implanted mice with EAC showed decreased activities of antioxidants (SOD, CAT, GR, GST and TAC) in comparison with normal animals. On the other hand, there is a significant increase in the enzymatic and

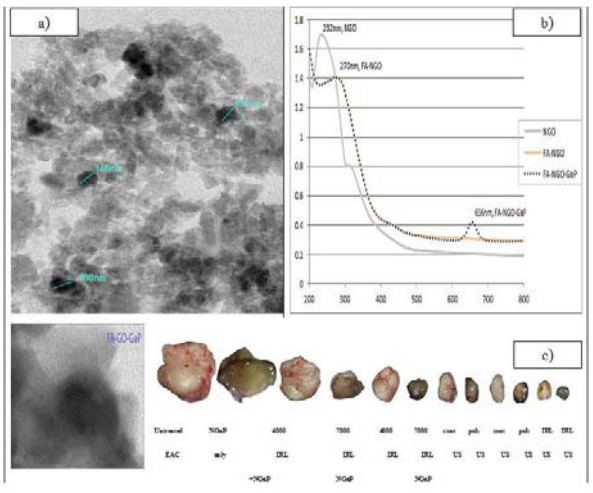

Figure 1: (a) TEM of FA-GO-GaP nanoparticle, (b) UV-vis spectra of GO, FA-GO and (c) FA-GO-GaP and the effect of IRL at different frequencies, US continuous/ pulsed and combined modalities on the tumor volume (mm3) for untreated and NGaP groups.

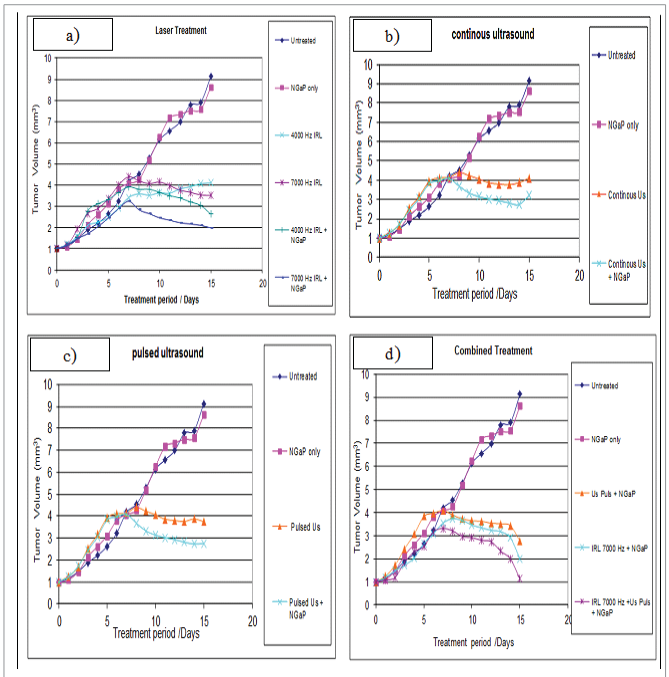

Figure 2: (a) The effect of IRL at different frequencies, (b), (c) US continuous/ pulsed and (d) Combined modalities on the tumor volume (mm3) for untreated and NGaP treated groups during treatment period

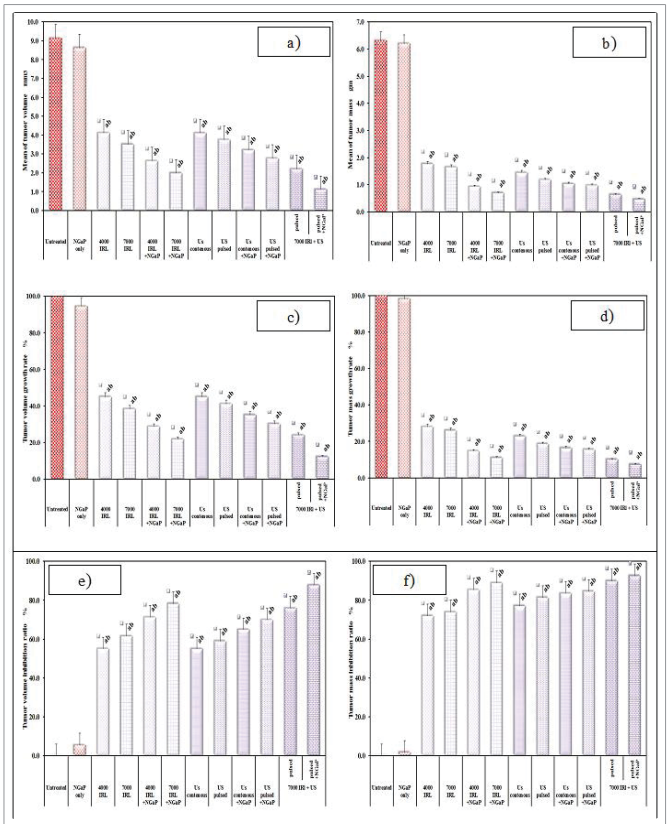

Figure 3: The effect of IRL at different frequencies US continuous/ pulsed and combined modalities on (a) the tumor volume (mm3), (b) tumor volume growth rate (%), (c) tumor volume inhibition ratio (%), (d) tumor mass (gm), (e) tumor mass growth rate (%), (f) tumor mass inhibition ratio (%) for untreated and NGaP treated groups. F: value for ANOVA test (TV (mm3): 56.887 $p < 0.001$*; TM (gm): 29.819 $p < 0.001$*). a: significant with EAC group; b: significant with NGaP only group; *: Statistically significant at p = 0.05.

non-enzymatic antioxidant guard in the groups irradiated with IRL or US or both with NGaP when compared with cancer control group or with treated mice without activation of NGaP.

Kidney and liver biomarkers

The renal function tests, namely; creatinine and urea, were estimated. The EAC caused a significant increase in the serum urea and creatinine levels in the studied groups. On the other hand the NGaP caused decrease in the levels of serum creatinine and urea which is probably an indication of renal protection (Figure 5). This also confirms the protective role of NGaP against renal toxicity. Also the hepatic function tests, ALT, AST and GGT, were estimated. The EAC caused a significant increase in the serum activities of ALT, AST and GGT of the tumor treated groups. However, in the EAC treated groups with NGaP a decrease in serum levels of ALT, AST, and GGT, were observed which is an indication of the hepatoprotection by NGaP, i.e., this confirms the protective role of NGaP against hepatotoxicity.

Histological evaluation

The histological evaluation revealed that all tumors from the group of mice bearing tumor without treatment working as a control group were highly malignant cells and the tumors showed 5-10% necrosis. Group of mice bearing tumor treated with (NGaP) only the similar percentage as only EAC group due to NGaP inactivation, Group of mice bearing tumor treated with 4000Hz, 7000Hz IRL only, showed

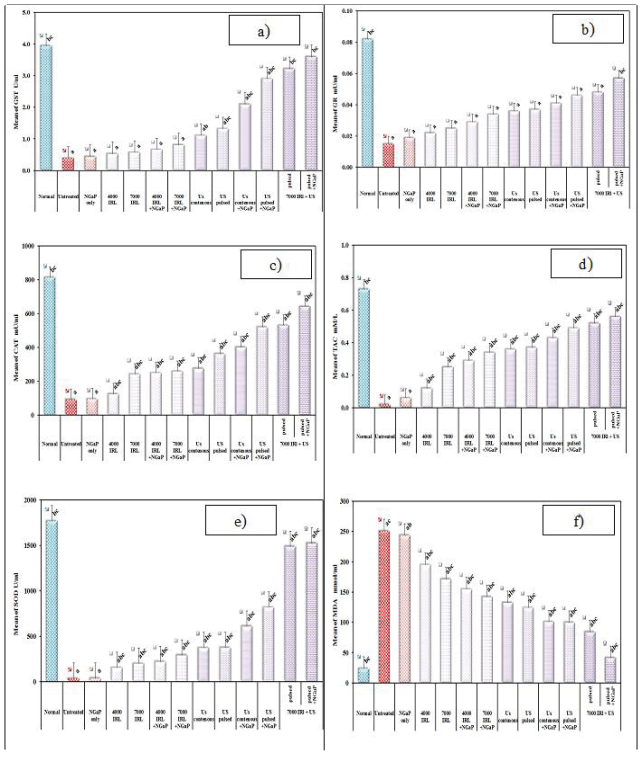

Figure 4: The effect of IRL at different frequencies US continuous/ pulsed and combined modalities on antioxidants activities, capacities and MDA [(a) GST, (b) GR, (c) CAT, (d) TAC, (e) SOD, (f) MDA] for untreated and NGaP treated groups. F: Value for ANOVA test (GST (U/ ml): 49.434 $p < 0.0001$*; GR (mU/ ml): 9.716 $p < 0.001$*; CAT (mU/ ml): 1576 $p < 0.001$*; TAC (mM/ L): 125.9 $p < 0.001$*; SOD (U/ ml): 28320 $p < 0.001$* and MDA (nmol/ ml): 1900 $p < 0.001$*). a: Significant with normal group; b: Significant with EAC group; c: Significant with NGaP group; *: Statistically significant at $p = 0.05$; data was expressed by using mean ±SD.

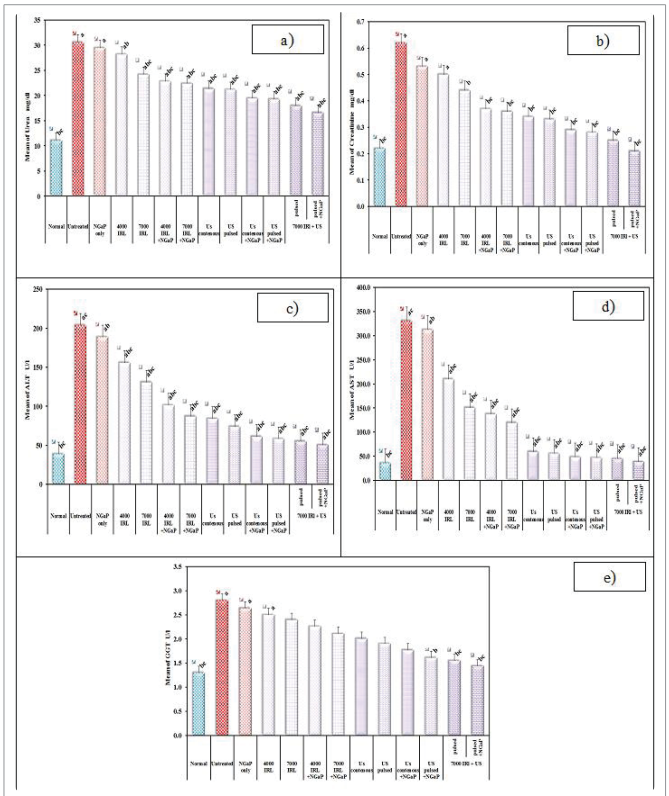

Figure 5: The effect of IRL at different frequencies, US continuous/ pulsed and combined modalities on renal [(a) urea, (b) creatinine] and hepatic [(c) ALT, (e) GGT] biomarkers for untreated and NGaP treated groups. F: Value for ANOVA test (Urea (mg/ dl): 234.122 $p < 0.001$*; Creatinine (mg/ dl): 6.392 $p < 0.001$*; ALT (U/ l): 413.9 $p < 0.001$*; AST (U/ l): 7745 $p < 0.001$* and GGT (U/ l): 4.429 $p < 0.001$*). a: Significant with normal group; b: Significant with EAC group; c: Significant with NGaP group; *: Statistically significant at $p = 0.05$; Data was expressed by using mean ±SD.

significant areas of necrosis (40- 55% respectively). In the group of mice injected IP with (NGaP) then the tumor site were irradiated to 4000Hz, 7000Hz showed significant areas of necrosis (56-67% respectively). Group of mice bearing tumor treated with continuous and pulsed ultrasound showed significant areas of necrosis (55- 60% respectively). The group of mice injected IP with (NGaP), then the tumor site was irradiated to continuous and pulsed ultrasound the areas of necrosis (65- 75% respectively), when compared with EAC untreated group. In case of two combination groups, mice bearing tumor treated 7000Hz followed by pulsed ultrasound only, and mice bearing tumor injected IP with (NGaP) then tumor site was irradiated to 7000Hz, followed by pulsed ultrasound, large foci of necrosis areas (80-82% respectively) were present which were distinctly appeared (Figure 6).

Osteopontin gene expression

Amplification of osteopontin gene expression in breast tissues of all studied groups using RT-PCR is shown in figure 7. PCR products were separated on 2% agarose gel electrophoresis. Products for osteopontin and GADPH gene expression were at 305 and 530bp respectively. Lane (a) is the molecular weight marker (50bp DNA ladder). All samples were positive to GADPH gene expression. Samples of lanes (1-3), lanes (4-6), lanes (7-9), and lanes (10-12) showed positive bands for osteopontin gene expression with different intensity; of EAC cancerous untreated group, EAC bearing group treated with laser, EAC bearing group treated with ultrasound,

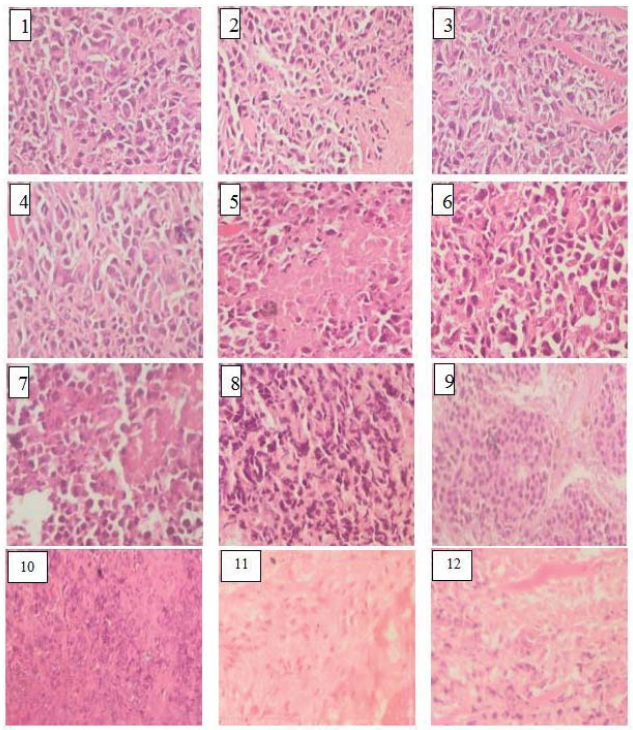

Figure 6: The effect of 4000 Hz IRL in absence of NGaP [necrosis 40%] (3), 7000 Hz IRL in absence of NGaP [necrosis 55%] (4), 4000 Hz IRL in presence of NGaP [necrosis 63%] (5), 7000 Hz IRL in presence of NGaP [necrosis 73%] (6), continuous US in absence of NGaP [necrosis 55%] (7), pulsed US in absence of NGaP [necrosis 60%] (8), continuous US in presence of NGaP [necrosis 72%] (9), pulsed US in presence of NGaP [necrosis 78%] (10), combined modalities IRL/ US in absence of NGaP [necrosis 80%] (11), and combined modalities IRL/ US in presence of NGaP [necrosis 92%] (12) on cellular level. [(Untreated EAC implanted group without any treatment [necrosis 10%], (2) NGaP treated group without activation [necrosis 12%]], Hematoxylin and eosin stain (H & E X 400).

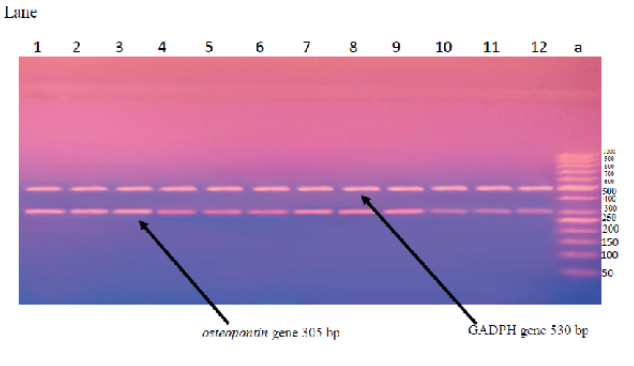

Figure 7: Osteopontin and GADPH-PCR products separated on 2% agarose gel electrophoresis. Products for osteopontin and GADPH gene expression were at 305 and 530 bp respectively. Lanes (1-3): Untreated EAC group; lanes (4-6): The effect of IRL at frequency (7000 Hz) in presence of NGaP; lanes (7-9): US pulsed in presence of NGaP and lanes (10-12): Combined modalities in presence of NGaP; positive bands with different intensity of osteopontin gene expression.

EAC bearing group treated with combined laser and ultrasound, respectively in presence of nano-GaP.

DISCUSSION

In the present work, nano-GaP as sono-photosensitizer, IR laser photodynamic therapy and sonodynamic therapy were employed to investigate whether alone or combined together, could be safely administered, provide an increased local tumor cytotoxic response and represents a promising approach in cancer therapy.

The MDA level is used as an indicator of oxidative stress, indicating an increasing interest in studying the role that lipid peroxidation played in the development of cancer. A low-molecular-weight aldehyde MDA is generated from free radical attack on polyunsaturated fatty acids [15,16].

The probable cause of a high level of serum lipid peroxide in cancer may be due to a defective antioxidant system that leads to accumulation of lipid peroxides in the cancerous tissues followed by secretion in the bloodstream [17]. MDA is a product of high-toxic cytotoxic aldehydes of lipid peroxidation. It is said to inhibit protective enzymes. Thus, they can have both mutagenic and carcinogenic effects [18].

In our study, the increase in lipid peroxidation was recorded during EAC which known with its carcinogenicity. All groups injected with EAC, have a statistical significant elevation in the levels of MDA as compared to the control group animals. The inhibition of peroxidation by nano-GaP is mainly attributed to the scavenging of the reactive free radicals involved in the peroxidation [19]. Animals in groups injected with nano-GaP as a treatment showed significantly low levels of MDA, compared to animals not treated with nano-GaP. This verifies the anti-lipid peroxidative role of nano-GaP by its ability to scavenge free radical generation.

For the purpose of preventing cellular damage caused by ROS, there is a lot of anti-oxidant defense system. The antioxidant defense system may detect ROS, which plays an important role in the initiation of lipid peroxidation, thus playing a protective role in the development of cancer [20]. This defense system works through enzymatic (including SOD, GPx, GST and CAT) and non-enzymatic components (mainly GSH) [21,22]. SOD is the basic step of the defense mechanism in an antioxidant system against oxidative stress, because it breaks down the superoxide anion (O2) into O2 and H_2O_2. Gpx and catalase can delete H_2O_2 and convert it to harmless by-products, thereby providing protection against ROS [23].

Also, GPX has a high strength in neutralizing reactivated free radicals in response to oxidative stress and detoxification of peroxides and hydroperoxides that lead to GSH oxidation [24]. Moreover, GST stimulates the coupling of functional groups of GSH atoms to electrophilic xenobiotics, leading to elimination or conversion of xenobiotic-GSH conjugate [25]. In such an interaction, GSH is oxidized into GSSG, which can be reduced to GSH by GR with NADPH consumption [26]. GSH is the most important non-enzymatic antioxidant in mammalian cells [27]. GSH is said to be involved in many cellular processes including detoxification of internal and external compounds and effectively protects cells against the harmful effects of oxidative stress by removing free radicals, removing H_2O_2, and suppressing lipid peroxidation [28].

In the present study, the EAC bearing mice showed decreased activities of antioxidants (SOD, CAT, GR, GST and TAC) in comparison with control animals. The present data are consistent with previous findings [29,30]. Pradeep, et al. [30] reported that such subsequent lower in the antioxidant defense is due to the low expression of these antioxidants during mammary gland damage. On the other hand, there is a significant increase in the enzymatic and

non-enzymatic antioxidant guard in the animals which carried the EAC when treated with nano-GaP, US and/or IRL when compared to the control group. This increase is due to the ability of nano-GaP to prevent the formation of free radicals, enhance the endogenous antioxidant activity beyond its free radical scavenging property and the reduction of EAC lipoperoxide formation [31].

The increase in the activities of the antioxidant enzymes in the nano-GaP treated mice compared to control group indicates its effect [32-41]. In this work, a statistically significant negative correlation between antioxidant activities and plasma mean levels of MDA was observed. The increased MDA level could be explained by defect in the antioxidant system with accumulation of lipid peroxides in the tumor as reported by Kumaraguruparan, et al. [41]. Furthermore, Sener, et al. found statistically significant decreased total antioxidant capacity with significantly increased serum MDA levels in EAC group compared to control group [42].

Urea and creatinine are metabolic products that are cleaned of the blood circulation by the kidneys to prevent their accumulation. Increasing serum levels of these substances is an indication of kidney function loss [43,44]. Data from this study suggest that mice groups implanted with EAC caused a loss of renal function compared with normal mice group and this is consistent with previous reports [45,46]. The urea and creatinine, biomarkers of renal function, were assessed in this study. It was observed in the current study that nano-GaP ameliorated the levels of serum urea and creatinine which is a marker of renal protection. This also indicates the protective role of nano-GaP against mice groups implanted with EAC which induced renal dysfunction.

The liver is implicated in the biotransformation of drugs and toxicants. The serum level of bilirubin and activities of the ALT, AST, ALP, and GGT liver enzymes, are considered reliable indices of hepatotoxicity [47,48]. Hepatocellular injury give rise to increase in serum ALT and AST [49]. Bilirubin is associated with liver, intestines, and spleen while ALP and GGT are associated with the cell membrane [50]. Serum bilirubin and activities of ALP and GGT increased in hepatobiliary injury [50]. The ALT, AST and GGT, biomarkers of hepatic function, were considered in this study. In this study, mice groups implanted with EAC caused increase in serum of ALT, AST and GGT activities. ALT and AST are present in the hepatocytes cytoplasm and mitochondria [51]. In this study, treatment with nano-GaP protected against increase in serum of ALT, AST, and GGT levels, which is an indication of hepato-protection by nano-GaP. This also confirms the protective role of nano-GaP against hepato-dysfunction.

In current work, study molecular study of osteopontin gene expression as a molecular diagnostic and prognostic markers for breast cancer revealed that there was a significantly negative correlation between modality of treatment and osteopontin gene expression in presence of sensitizer in treated groups while a positive correlation between osteopontin gene expression and cancer progression in the untreated cancerous group. Osteopontin gene expression significantly lower in mice groups treated with sonophoto treatment [in presence of nano-GaP] than those treated with photo- or sono- treatment only [in presence of nano-GaP alone] followed by photo- or sono- treatment only [in absence of nano-GaP alone] while the highest expression was among the untreated cancerous group. The present results further support that molecular detection of osteopontin gene expression using RT-PCR could be used as a diagnostic and prognostic predictor of breast cancer and was in agreement with other studies done by other authors [52-57].

Finally, it can be concluded that the present study opened new trends for cancer treatment therapy that needs to be further verified. The study gave profound results involving the use of sono-photo-dynamic modality employing exposure to infra-red laser and ultrasound with (pulsed and continuous) in combination with nano-GaP as a sono-photo sensitizer for treating Ehrlich tumor inoculated to mice as an experimental animals. The possible application of nano-carrier-sono-photo-dynamic therapy as in vivo anti-malignancy can open new line of research for modern cancer therapy that needs to be further investigated. Nanomaterial with their effective drug delivery great potential for can permit the feasibility of targeted therapy for disease treatment that needs further research for optimizing and maximizing benefits. Conjugated nanomaterial therapy can potentially provide a very valuable application for amplifying the benefits of photodynamic therapy. Response can be improved utilizing sonodynamic targeted therapy to treat deep or multiple lesions simultaneously. Further research is required to validate this novel therapy to prove feasibility and safety of application.

CONCLUSION

The present study gave profound results involving the use of sono-photo-dynamic modality employing exposure to infra-red laser and ultrasound with (pulsed and continuous) in combination with nano-GaP as a sono-photo sensitizer for treating implanted Ehrlich tumor in mice as an experimental animals showing promising results for cancer treatment.

RECOMMENDATION

The present study opened new trends for cancer treatment therapy that needs to be further verified. It is strictly recommended to conduct further experimental protocols aiming to safely apply this up-to-date modality on human and recording other biochemical and/or biophysical parameter's variations.

References

1. Ferlay J, Soerjomataram I, Ervik M, Dikshit R, Eser S, Mathers C, et al. GLOBOCAN 2012: estimated cancer incidence, mortality and prevalence worldwide in 2012 v1.0. IARC Cancer Base No. 11. International Agency for Research on Cancer, Lyon; 2013. https://goo.gl/x3ofuA
2. Bray F, Jemal A, Grey N, Ferlay J, Forman D. Global cancer transitions according to the Human Development Index (2008-2030): a population-based study. Lancet Oncol. 2012; 13: 790-801. https://goo.gl/MZnJQv
3. Torre LA, Siegel RL, Ward EM, Jemal A. Global cancer incidence and mortality rates and trends-an update. Cancer Epidemiol Biomarkers Prev. 2016; 25: 16-27. https://goo.gl/UwNfjp
4. Urruticoechea A, Alemany R, Balart J, Villanueva A, Viñals F, Capellá G. Recent advances in cancer therapy: an overview. Curr Pharm Des. 2010; 16: 3-10. https://goo.gl/bgWXs5
5. Mehta BM, Patel VK, Thakkar SG. New generation of cancer treatment: immunotherapy. J Genet Mol Biol. 2017; 1: 1-14. https://goo.gl/kg2SgS
6. Castano AP, Demidova TN, Hamblin MR. Mechanisms in photodynamic therapy: part one-photosensitizers, photochemistry and cellular localization. Photodiagnosis Photodyn Ther. 2004; 1: 279-293. https://goo.gl/bHKkz1
7. Mroz P, Yaroslavsky A, Kharkwal GB, Hamblin MR. Cell death pathways in photodynamic therapy of cancer. Cancers (Basel). 2011; 3: 2516-2539. https://goo.gl/YqVwpm
8. Brodin NP, Guha C, Tomé WA. Photodynamic therapy and its role in

combined modality anticancer treatment. Technol Cancer Res Treat. 2015; 14: 355-368. https://goo.gl/QLy17G

9. Costley D, McEwan C, Fowley C, McHale AP, Atchison J, Nomikou N, et al. Treating cancer with sonodynamic therapy: a review. Int J Hyperthermia. 2015; 31: 107-117. https://goo.gl/NYEDTD

10. Su X, Wang P, Yang S, Zhang K, Liu Q, Wang X. Sonodynamic therapy induces the interplay between apoptosis and autophagy in K562 cells through ROS. Int J Biochem Cell Biol. 2015; 60: 82-92. https://goo.gl/HhwWgX

11. McEwan C, Owen J, Stride E, Fowley C, Nesbitt H, Cochrane D, et al. Oxygen carrying microbubbles for enhanced sonodynamic therapy of hypoxic tumours. J Control Release. 2015; 203: 51-56. https://goo.gl/7PvB2m

12. Wan GY, Liu Y, Chen BW, Liu YY, Wang YS, Zhang N. Recent advances of sonodynamic therapy in cancer treatment. Cancer Biol Med. 2016; 13: 325-338. https://goo.gl/Ja5p4r

13. Miyoshi N, Kundu SK, Tuziuti T, Yasui K, Shimada I, Ito Y. Combination of sonodynamic and photodynamic therapy against cancer would be effective through using a regulated size of nanoparticles. Nanosci Nanoeng. 2016; 4: 1-11. https://goo.gl/cTBii5

14. Abd El-Kareem SA, Abd Elsamie GH, Abd-Alkareem AS. Sono-photodynamic modality for cancer treatment using bio-degradable bio-conjugated sonnelux nanocomposite in tumor-bearing mice: activated cancer therapy using light and ultrasound. Biochem Biophys Res Commun. 2018; 503: 1075-1086. https://goo.gl/HGmyrg

15. Rao CSS, Kumari DS. Changes in plasma lipid peroxidation and the antioxidant system in women with breast cancer. Int J Basic Appl Sci. 2012; 1: 429-438. https://goo.gl/UsJkkA

16. Kumaraguruparan R, Subapriya R, Viswanathan P, Nagini S. Tissue lipid peroxidation and antioxidant status in patients with adenocarcinoma of the breast. Clin Chim Acta. 2002; 325: 165-170. https://goo.gl/DKVpfS

17. Ziech D, Franco R, Georgakilas AG, Georgakila S, Malamou-Mitsi V, Schoneveld O, et al. The role of reactive oxygen species and oxidative stress in environmental carcinogenesis and biomarker development. Chem Biol Interact. 2010; 188: 334-339. https://goo.gl/A8ck85

18. Naser B, Bodinet C, Tegtmeier M, Lindequist U. Thuja occidentalis (Arbor vitae): a review of its pharmaceutical, pharmacological and clinical properties. Evid Based Complement Alternat Med. 2005; 2: 69-78. https://goo.gl/V3vn5w

19. Lopez-Lázaro M. Anticancer and carcinogenic properties of curcumin: considerations for its clinical development as a cancer chemo preventive and chemotherapeutic agent. Mol Nut Food Res. 2008; 52: 103-127. https://goo.gl/9Q9AxT

20. Zhang CL, Zeng T, Zhao XL, Yu LH, Zhu ZP, Xie KQ. Protective effects of garlic oil on hepatocarcinoma induced by Nnitrosodiethylamine in rats. Int J Biological Sci. 2012; 8: 363-374. https://goo.gl/zWvg7W

21. Chen B, Ning M, Yang G. Effect of paeonol on antioxidant and immune regulatory activity in hepatocellular carcinoma rats. Molecules. 2012; 17: 4672-4683. https://goo.gl/dfo5fs

22. Vásquez-Garzón V, Arellanes-Robledo J, García-Román R, Aparicio-Rautista DI, Villa-Treviño S. Inhibition of reactive oxygen species and pre-neoplastic lesions by quercetin through an antioxidant defense mechanism. Free Radic Res. 2009; 43: 128-137. https://goo.gl/bUJhfG

23. Usunomena U, Ademuyiwa A, Tinuade O, Uduenevwo F, Martin O, Okolie N. N-Nitrosodimethylamine (NDMA), liver function enzymes, renal function parameters and oxidative stress parameters: a review. Br J Pharmaco Toxicol. 2012; 3: 165-176. https://goo.gl/hyBZ2e

24. Rao GM, Rao CV, Pushpangadan P, Shirwaikar A. Hepatoprotective effects of rubiadin, a major constituent of Rubia cordifolia Linn. J Ethnopharmacol. 2006; 103: 484-490. https://goo.gl/drdo4D

25. Revathi R, Manju V. The effects of Umbelliferone on lipid peroxidation and antioxidant status in diethylnitrosamine induced hepatocellular carcinoma. J Acute Medicine. 2013; 3: 73-82. https://goo.gl/skShk8

26. Wu G, Fang, YZ, Yang S, Lupton JR, Turner ND. Glutathione metabolism and its implications for health. J Nutr. 2004; 134: 489-492. https://goo.gl/j6k7bm

27. Blair IA. Endogenous glutathione adducts. Curr Drug Metab. 2006; 7: 853-872. https://goo.gl/nwzLMx

28. Ghosh D, Choudhury ST, Ghosh S, Mandal AK, Sarkar S, Ghosh A, et al. Nanocapsulated curcumin: oral chemopreventive formulation against diethylnitrosamine induced hepatocellular carcinoma in rat. Chem Biol Interact. 2012; 195: 206-214. https://goo.gl/8PgJ4V

29. Rajeshkumar N, Kuttan R. Inhibition of N-nitrosodiethylamine induced hepatocarcinogenesis by Picroliv. J Exp Clin Cancer Res. 2000; 19: 459-465. https://goo.gl/CydnBC

30. Pradeep K, Mohen, CV, Gobian K, Karthikeyan S. Silymarin modulates the oxidant-antioxidant imbalance during diethylnitrosamine induced oxidative stress in rats. Eur J Pharmacol. 2007; 560:110-116. https://goo.gl/Yqw8CD

31. Ren W, Qiao Z, Wang H, Zhu L, Zhang L. Flavonoids: promising anticancer agents. Med Res Rev. 2003; 23: 519-534. https://goo.gl/j7QZMj

32. Bemis D, Capodice J, Gorroochurn P, Katz A, Buttyan R. Anti-prostate cancer activity of a beta-carboline alkaloid enriched extract from Rauwolfia vomitoria. Int J Oncol. 2006; 29: 1065-1073. https://goo.gl/sCEj85

33. Grippo AA, Capps K, Rougeau B, Gurley BJ. Analysis of flavonoid phytoestrogens in botanical and ephedra-containing dietary supplements. Ann Pharmacother. 2007; 41: 1375-1382. https://goo.gl/bBaJwm

34. Jiang J, Hu C. Evodiamine: a novel anti-cancer alkaloid from Evodiarutaecarpa. Molecules. 2009; 14: 1852-1859. https://goo.gl/R5pVnX

35. Kabashima H, Miura N, Shimizu M, Shinoda W, Wang X, Wang Z, et al. Preventive impact of alkaloids with anti-cancer effect extracted from natural herb and the derivatives. Webmed Central. 2010; 1: 1-19. https://goo.gl/zfZ4Kh

36. Thoppil R, Bishayee A. Terpenoids as potential chemopreventive and therapeutic agents in liver cancer. World J Hepatol. 2011; 3: 228-249. https://goo.gl/cZv2ux

37. Kuno T, Tsukamoto T, Hara A, Tanaka T. Cancer chemoprevention through the induction of apoptosis by natural compounds. J Biophys Chem. 2012; 3: 156-173. https://goo.gl/MK7PFg

38. Haghiac M, Walle T. Quercetin induces necrosis and apoptosis in SCC-9 oral cancer cells. Nutr Cancer. 2005; 53: 220-231. https://goo.gl/YPya3r

39. Priyadarsini R, Murugan R, Maitreyi S, Ramalingam K, Karunagaran D, Nagini S. The flavonoid quercetin induces cell cycle arrest and mitochondria-mediated apoptosis in human cervical cancer (HeLa) cells through p53 induction and NF-jB inhibition. Eur J Pharmacol. 2010; 649: 84-91. https://goo.gl/Dt78pg

40. Bishayee K, Ghosh S, Mukherjee A, Sadhukhan R, Mondal JK, Khuda-Bukhsh AR. Quercetin induces cytochrome-c release and ROS accumulation to promote apoptosis and arrest the cell cycle in G2/ M, in cervical carcinoma: signal cascade and drug-DNA interaction. Cell Prolif. 2013; 46: 153-163. https://goo.gl/XDgmCM

41. Kumaraguruparan R, Subapriya R, Kabalimoorthy J, Nagini S. Antioxidant profile in the circulation of patients with fibroadenoma and adenocarcinoma of the breast. Clin Biochem. 2002; 35: 275-279. https://goo.gl/Rgvjdh

42. Sener D, Gönenç A, Akinci M, Torun M. Lipid peroxidation and total antioxidant status in patients with breast cancer. Cell Biochem Funct. 2007; 25: 377-382. https://goo.gl/RpGpM2

43. Han WK, Bonventre J. Biologic markers for the early detection of acute kidney injury. Curr Opin Crit Care. 2004; 10: 476-482. https://goo.gl/1LTRRv

44. George G, Wakasi M, Egoro E. Creatinine and urea levels as critical markers in end-stage renal failure. Research and Review. J Med Heal Sci. 2014; 3: 41-44.

45. Paliwal R, Sharma V, Pracheta, Sharma S, Yadav S, Sharma SH. Antinephrotoxic effect of administration of Moringaoleifera Lam. in amelioration

of DMBA-induced renal carcinogenesis in Swiss albino mice. Biol Med. 2011; 3: 27-35. https://goo.gl/WA9Wiq

46. Sharma V, Paliwal R, Janmeda P, Sharma SH. The reno-protective efficacy of Moringaoleifera pods on xenobiotic enzymes and antioxidant status against 7,12-dimethylbenz[a]anthracene exposed mice. J Chin Integr Med. 2012; 10: 1171-1178.

47. Boone L, Meyer D, Cusick P, Ennulat D, Bolliger AP, Everds N. Selection and interpretation of clinical pathology indicators of hepatic injury in preclinical studies. Vet Clin Pathol. 2005; 34: 182-188. https://goo.gl/s547Hc

48. Singh A, Bhat TK, Sharma OM. Clinical biochemistry of hepatotoxicity. J Clinic Toxicol. 2011; 4: 1-19. https://goo.gl/VcTHJW

49. Ozer J, Ratner M, Shaw M, Bailey W, Schomaker S. The current state of serumbiomarkers of hepatotoxicity. Toxicology. 2008; 245: 194-205. https://goo.gl/XqpoBE

50. Ramaiah S. A toxicologist guide to the diagnostic interpretation of hepatic biochemical parameters. Food Chem Toxicol. 2007; 45: 1551-1557. https://goo.gl/jJBjwM

51. Amacher D. A toxicologist's guide to biomarkers of hepatic response. Hum Exp Toxicol. 2002; 21: 253-262. https://goo.gl/vozyfa

52. Unni E, Kittrell FS, Singh U, Sinha R. Osteopontin is a potential target gene in mouse mammary cancer chemoprevention by Se-methylselenocysteine. Breast Cancer Res. 2004; 6: 586-592. https://goo.gl/kD7xM9

53. Weber GF. The metastasis gene osteopontin: a candidate target for cancer therapy. Biochim Biophys Acta. 2001; 1552: 61-85. https://goo.gl/DvQqS1

54. Bellahcene A, Castronovo V, Ogbureke KU, Fisher LW, Fedarko NS. Small Integrin-Binding Ligand N-Linked Glycoproteins [SIBLINGs]: multifunctional proteins in cancer. Nat Rev Cancer. 2008; 8: 212-226. https://goo.gl/KWUrBd

55. Wai PY, Kuo PC. Osteopontin: regulation in tumor metastasis. Cancer Metastasis Rev. 2008; 27: 103-118. https://goo.gl/NPW4mb

56. El Tanani, MK, Campbell FC, Kurisetty V, Jin D, McCann M, Rudland PS. The regulation and role of osteopontin in malignant transformation and cancer. Cytokine Growth Factor Rev. 2006; 17: 463-474. https://goo.gl/bonruw

57. Hedley BD, Welch DR, Allan AL, Al-Katib, W, Dales DW, Postenka CO, et al. Downregulation of osteopontin contributes to metastasis suppression by breast cancer metastasis suppressor 1. Int J Cancer. 2008; 123: 526-534. https://goo.gl/QZ5jtv